



Sharif University of Technology

Scientia Iranica

Transactions B: Mechanical Engineering

www.sciencedirect.com



Research note

Effects of wing geometry on wing-body-tail interference in subsonic flow

A.R. Davari^{a,*}, M.R. Soltani^b, F. Askari^b, H.R. Pajuhande^a

^a Department of Mechanical and Aerospace Engineering, Islamic Azad University, Science and Research Branch, Poonak, Tehran, P.O. Box 14155-4933, Iran

^b Department of Aerospace Engineering, Sharif University of Technology, Tehran, P.O. Box 11155-9567, Iran

Received 17 February 2010; revised 7 December 2010; accepted 24 April 2011

KEYWORDS

Tip vortex;
Interference;
Forebody vortex shedding.

Abstract Extensive wind tunnel tests were performed on several wing-body-tail combinations in subsonic flow to study the effects of wing geometric parameters on the flow field over the tail. For each configuration, tail surface pressure distribution, as well as the velocity contour at a plane perpendicular to the flow direction behind the wing was measured. The results show a strong effect of wing to tail span ratio, as well as wing aspect ratio, on the flowfield downstream of the wing. For low sweep wings, as those considered here, wing and body interference effects on the tail are associated with the wing tip vortex and nose-body vortex.

© 2011 Sharif University of Technology. Production and hosting by Elsevier B.V.

Open access under [CC BY-NC-ND license](https://creativecommons.org/licenses/by-nc-nd/4.0/).

1. Introduction

The interference problem among the components of an airplane or missile has received considerable attention because of its importance in modern aircraft design. This importance is due to the interest in designs employing small wing to tail span. During the past decades, attempts have been made to develop accurate and suitable methods to investigate this problem. One of the earliest attempts to study and employ such methods is the work of Lennertz in 1934 [1]. His work was then verified and supported by the subsonic experimental data provided by Hopkins [2]. At supersonic speeds, some laborious methods were developed for computing the interference effects of the body on the load distribution of the wing and tail [3–5]. Another investigation to study the effects of the wing on the tail flow field in subsonic flow is that of Sliverstein [6], Sliverstein and

Katzoff [7]. For supersonic speeds, Morikawa [8] examined four limiting cases of zero and infinite aspect ratio for wing and tail. He showed that for equal wing and tail spans, the lift loss due to interference can be as large as the wing lift itself. Using the slender body theory, Lomax and Byrd [9] analyzed wing-tail interference for several swept wing configurations. Lagerstrom and Graham [10] developed a method based on the strip theory to determine tail loads due to a nonuniform downwash field.

Brebner [11] summarized the different control methods in aircraft, such as tail-control, canard control, jet reaction control, thrust vector control, etc., and investigated the body effects on the amount of wing downwash shed into the tail flow field at low angles of attack. He found that the body decreases downwash on the tail, which is known as the body upwash effect. Lesieutre [12] constructed a large experimental data bank from the aerodynamic behavior of several wing-body combinations at a vast range of Mach numbers, from 0.6 to 4.5. This data bank was then used to develop the Missile III engineering code. This code is capable of calculating interference effects for low aspect ratio fins [12–15].

Wing-tail interference effects are very important at high angles of attack and have a strong impact on the prediction accuracy of the usual engineering codes. Abney [16] in 2005 studied different configurations including several bodies, several wings, and some combinations of them, at high angles of attack and at a constant Mach number of 0.8. He examined the prediction accuracy of an engineering code for these configurations at high angles of attack [16].

The attempts made so far were mainly concentrated on determining wing-body-tail interference effects by calculation

* Corresponding author.

E-mail address: ardavari@srbiau.ac.ir (A.R. Davari).



Nomenclature

x	Chord wise distance measured from the tail leading edge
y	Span wise distance measured from the body surface
z	Vertical distance from the planform surface
c	Tail chord at root section
α	Angle of attack
AR	Wing aspect ratio
Δ	Wing leading edge sweep angle
c_p	Pressure coefficient

of the aerodynamic forces. This is essentially helpful in developing some relations to take care of these effects in calculating aerodynamic forces and moments.

In this paper, a comprehensive experimental study was conducted to obtain a physical insight into the impact of the wing on the tail flow field. Effects of various wings on the tail flow field were studied by measuring the tail pressure distribution. This is a helpful data bank for code verification and gives a physical feeling about the way a wing can communicate with the downstream lifting surface.

The results are helpful in airplane and projectile design, whereas the wing/tail spacing and wing to tail span ratio play an important role in the aerodynamic behavior of both wing and tail. The latter is especially of great importance in the stability and control of the vehicle. Using the provided data bank, one can easily see the impact of wing geometric parameters on the flow field over the tail. This can greatly improve the aerodynamic performance of planforms for various flying vehicles.

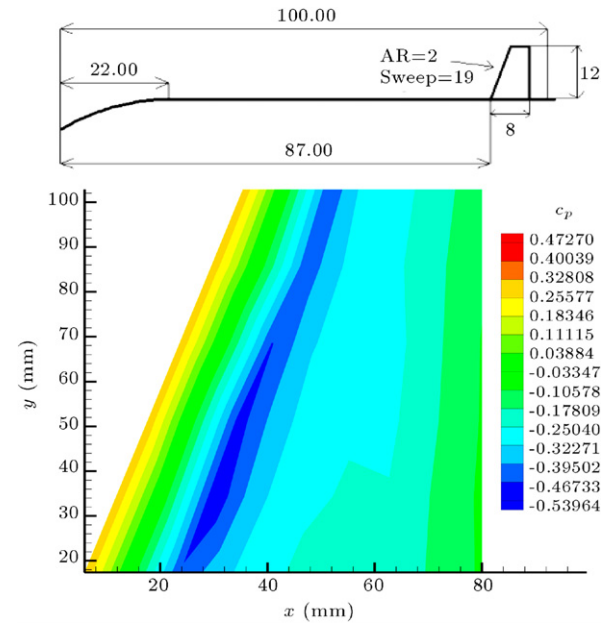
2. Model and experimental apparatus

The present experiments were conducted in a 80 by 80 cm subsonic wind tunnel at a constant velocity of 90 m/s. Six different wing–tail combinations were manufactured and tested to study the effects of wing geometric parameters on the flow field over the tail, at both small and high angles of attack. Table 1 summarizes the geometric characteristics of the configurations.

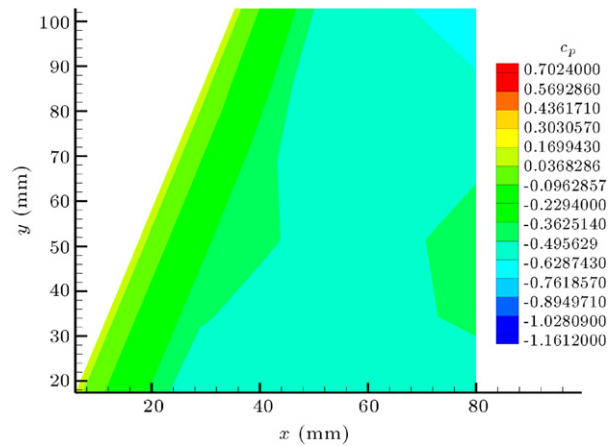
64 small pressure tabs were carefully drilled on both upper and lower surfaces of the tail, and the experiments consisted of measuring the tail surface pressure distribution using sensitive pressure transducers. In addition, the sectional velocity distribution at a plane normal to the flow direction downstream of the wing, at a position where the tail is installed, was measured using a 51 pressure probe rake. The data presented here are only for angles of attack of 5 and 30° for the same body and tail, T , combined with different wing geometries located upstream, TW1–TW5.

3. Results and discussions

The results of the present experiments consist of tail surface pressure, as well as velocity distribution downstream of the wing. Figure 1 shows the effects of angle of attack on the surface pressure field over the configuration designated by T in Table 1, i.e. the body tail configuration. At an angle of attack of 5°, a narrow high velocity, low pressure region is observed near the leading edge of the tail, which is a vortex dominated flow



(a) $\alpha = 5^\circ$.



(b) $\alpha = 30^\circ$.

Figure 1: Surface pressure distribution on body–tail alone configuration, T .

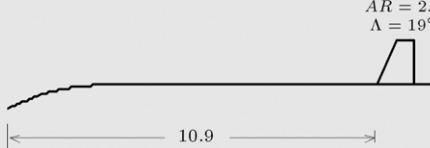
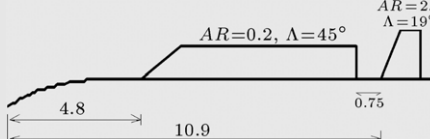
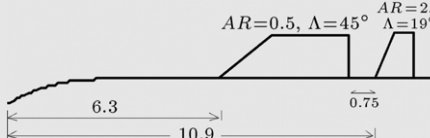
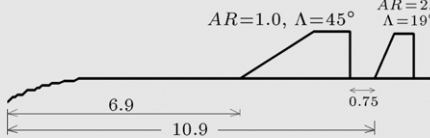
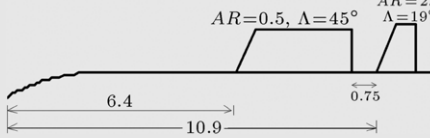
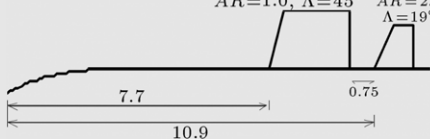
caused by the leading edge separation. Note that the flow re-attachment line on the tail at this angle of attack is at about the quarter chord, extending in the spanwise direction.

At an angle of attack of 30°, the separated flow region is prevailed over the entire tail surface (Figure 1). However, a weakly attached flow is still observed at the right corner near the tip, which seems to be due to the vortex shedding from the nose and body at this high angle of attack.

The picture is totally different when a wing is placed upstream of the tail. Figure 2 shows the tail surface pressure field when a wing of aspect ratio 0.2, with a 45° sweep angle, is located upstream of the tail. This configuration is denoted by TW1 in Table 1. At $\alpha = 5^\circ$, according to the velocity contours obtained downstream of the wing exactly at the position of the tail, a small wing tip vortex exists in the downstream flow field over the tail (Figure 2(a)).

The vortical flow pattern observed in Figure 1(a) has nearly disappeared in Figure 2(b), due to the dissipative nature of the wake of the wing, which increases the downwash seen by the

Table 1: Configurations considered in the present experiments.

Configuration designation	Schematic (All lengths are divided by the tail root chord)	Wing/tail span ratio
T		-
TW1		0.75
TW2		1.00
TW3		1.20
TW4		1.00
TW5		1.40

tail. However, the short low pressure streak near the tail tip is clearly due to the wing tip vortex, which imparts energy to the separated flow on the tail and causes it to reattach on the surface at the re-attachment line mentioned earlier.

The length of this low-pressure streak near the tip is approximately equal to the wing tip vortex diameter, verifying that the low-pressure region seen in Figure 2(b) is due to the wing tip vortex. It could be concluded that for this case, Figure 2(b), the presence of the wing deteriorates the flow field over the tail surface.

At $\alpha = 30^\circ$, the wing tip vortex has been fully developed and covers nearly the entire wing span. This vortex greatly affects the separated flow on the tail, seen in Figure 1(b), and reattaches it in the form of a thick suction zone (Figure 2(d)). Due to the small wing span, the tip vortex core is located outboard on the wing and the width of the low pressure region on the tail outboard is larger than the inboard position, forming an “Insect’s wing” shape (Figure 2(d)). This shape is due to the relatively strong and wide wake region of the wing, as observed in Figure 2(c).

Shown in Figure 3 is the pressure field on the tail surface, located downstream of another wing, having an aspect ratio of 0.5 and a sweep angle of 45° , designated by TW2. Returning to Figure 2, the tip vortex in the TW1 directly passes over the tail and affects its flow field, as seen from this figure. For the TW1, both the wing aspect ratio and the wing to tail span ratio are smaller than unity. However, for the TW2 case, the

wing to tail span ratio is exactly 1.0, and the wing aspect ratio is higher than that for the TW1. As a result, the tail surface remains unaffected by the wing tip vortex, while it proceeds downstream away from the tail. For this reason, the low-pressure streak observed in Figures 1(a) and 2(b) near the tail leading edge is disappeared in Figure 3(a) by the separated flow of the wing, which decreases the flow energy on the tail surface. Therefore, at an angle of attack of 5° , the flow field over the tail surface is almost separated (Figure 3(a)), while for the previous case, and at the same angle of attack, the situations were different.

Again, at $\alpha = 30^\circ$, the insect’s wing shape-streak has been formed on the tail surface, due to the combined effects of nose and forebody vortex shedding, as well as the spanwise growth of the wing tip vortex at this high angle of attack (Figure 3(b)).

Since the main source of the suction region on the tail for both TW1 and TW2 configurations is the same, i.e. the wing tip vortex with a small effect due to the body vortex shedding, the shape of this region on the tail at $\alpha = 30^\circ$ for these two configurations is also similar (Figures 2(d) and 3(b)).

In Figure 4, a different wing planform is placed upstream of the tail. This configuration is designated by TW3 and has the same sweep angle as those of the TW1 and TW2, but its aspect ratio is higher, i.e. the wing span is larger than that of the tail. In this case, neither at $\alpha = 5^\circ$ nor at $\alpha = 30^\circ$, the wing tip vortex effect is felt on the tail (Figure 4(a) and (b)).

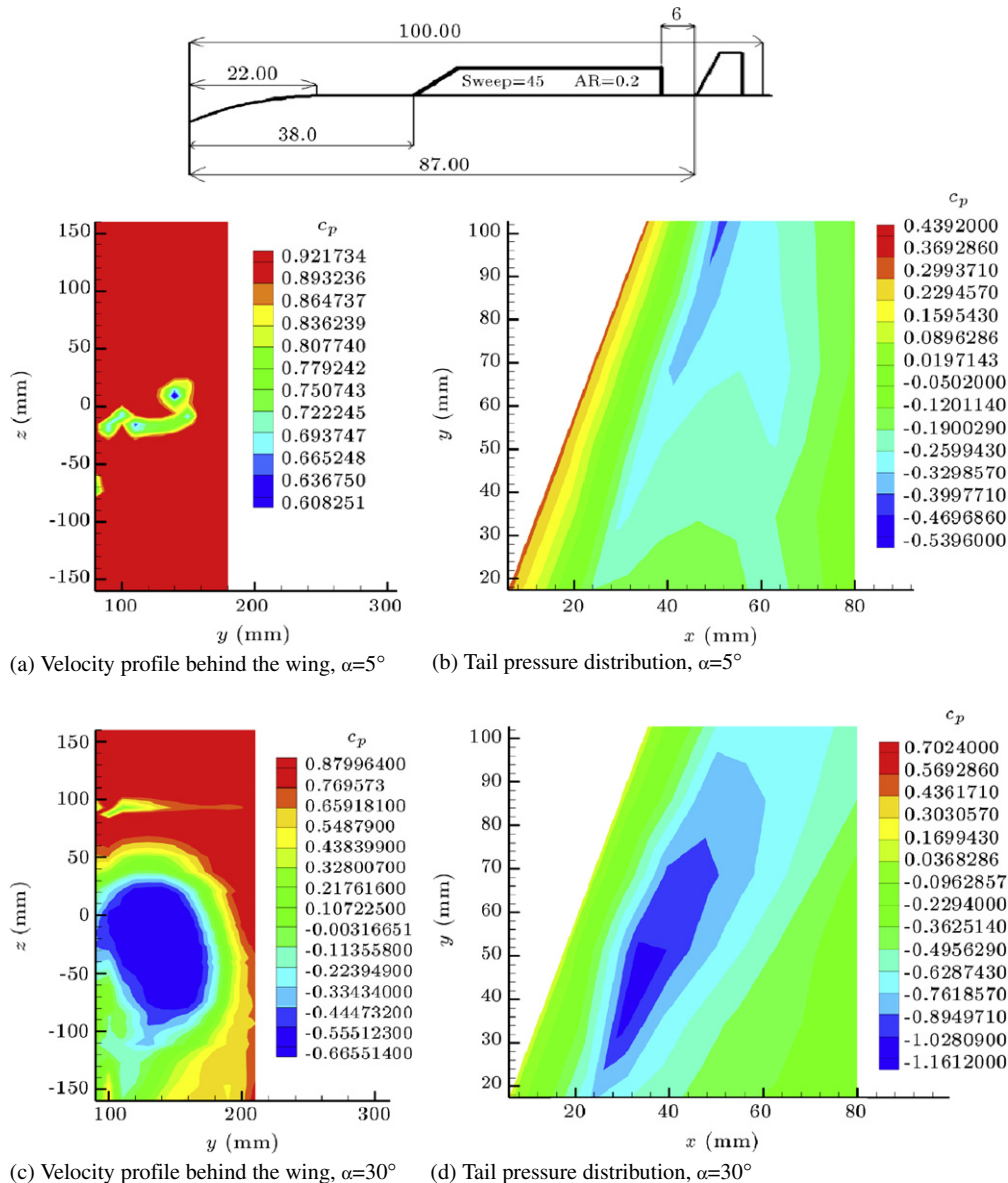


Figure 2: The flowfield downstream of the wing of TW1 configuration.

For TW3 at $\alpha = 5^\circ$, similar to TW1 and TW2, the suction region on the tail is disappeared due to the wake of the wing. However, at $\alpha = 30^\circ$, the shape of the low pressure field on the tail is completely different. The wing span for this configuration is not short enough to be fully covered by the wing tip vortex and affect the tail surface located downstream, as for the cases of TW1 and TW2. Thus the low pressure region on the tail in TW3 configuration is an indication of the nose and the body vortex shedding, not the wing flow field. As a result, the low pressure region, in contrast to the TW1 and the TW2 cases, is concentrated near the tail root at the junction of the tail and body.

Note that for the TW3 case, the low-pressure region is extended more in the chord wise direction (Figure 4(b)), compared to the similar cases of TW1 and TW2, indicating the different effects of the wing tip and nose-body vortices on the tail. They both energize the separated flow of the tail, caused by the wake of the wing. However, it seems that the tip vortex zone of action is at the tail outboard section, in the span wise

direction, while the body vortex mostly affects the tail inboard position, extending in the chord wise direction. According to the results, the body vortex energizes the flow and reattaches it to the tail surface, similar to the wing tip vortex effects.

The configuration shown in Figure 5, designated by TW4, consists of a wing with the same aspect ratio of TW2, but with a sweep angle of 21° . As in the cases of TW2 and TW3 shown in Figures 3 and 4, the wing exhibits nearly no favorable effect on the tail at $\alpha = 5^\circ$, due to high wing to tail span ratio and relatively high aspect ratio. The wing tip vortex line, as shown in Figure 5(b), is not close enough to the tail surface to impart any noticeable suction on it.

However, similar to the TW2 case shown in Figure 3, at $\alpha = 30^\circ$, the wing tip vortex plays an important role in re-establishing a low-pressure streak on the tail. Even though the configurations, TW4 and TW2, have the same wing aspect ratio, their wing sweep angles are different. The effects of this difference are observed by comparing Figure 3 with Figure 5. The difference is obviously in the spanwise distribution of the

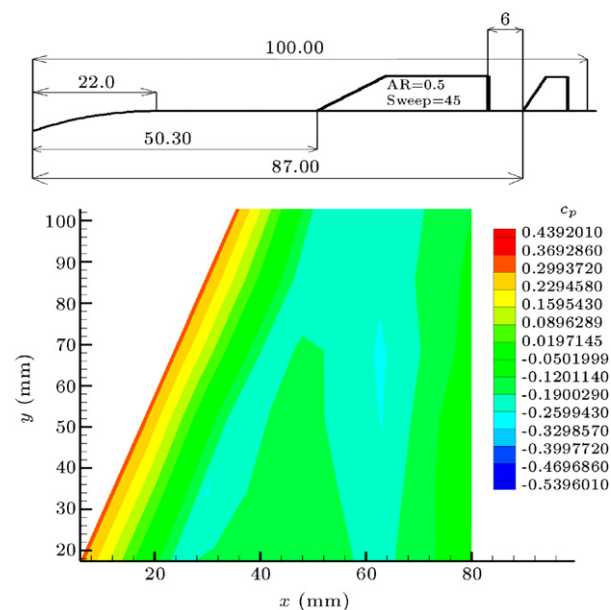
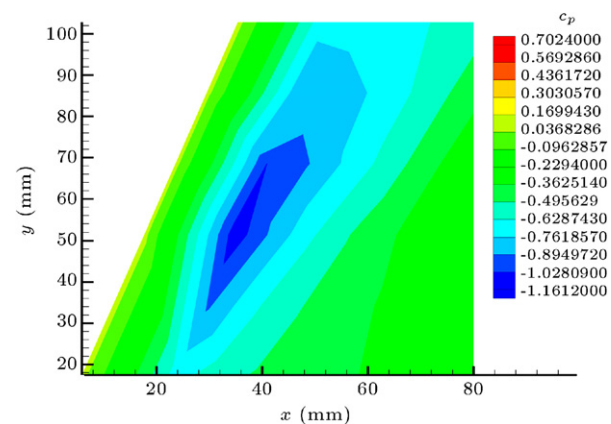
(a) $\alpha = 5^\circ$.(b) $\alpha = 30^\circ$.

Figure 3: The flowfield behind the TW2 configuration.

width of the low pressure streak. In Figure 3, the width of this region is very small near the root and increases toward the tip. This indicates that the effect of the wing tip vortex on TW2 is more pronounced than the body vortex shedding. However, for the TW4 configuration shown in Figure 5, the width of this region is nearly constant throughout the wing span, indicating equal contributions of wing tip vortex and body vortex shedding. As noted earlier, this difference is due to wing sweep angles, which have a direct impact on the formation and development of the leading edge vortex on the wing. The leading edge vortex seems to be effective on the tip vortex and its spanwise growth.

The effect of a higher aspect ratio and lower sweep angle wing, denoted by TW5, on the tail flow field is shown in Figure 6. Again, since both the wing aspect ratio and the wing to tail span ratio are high, no favorable effects of wing tip vortex on the tail at $\alpha = 5^\circ$ is felt, and the suction region on the tail, observed in Figure 1(a), has been deteriorated by the wake of the wing, as shown in Figure 6(a).

At a 30° angle of attack, the shape of the suction region on the tail for this configuration is similar to that of Figure 4 for TW3.

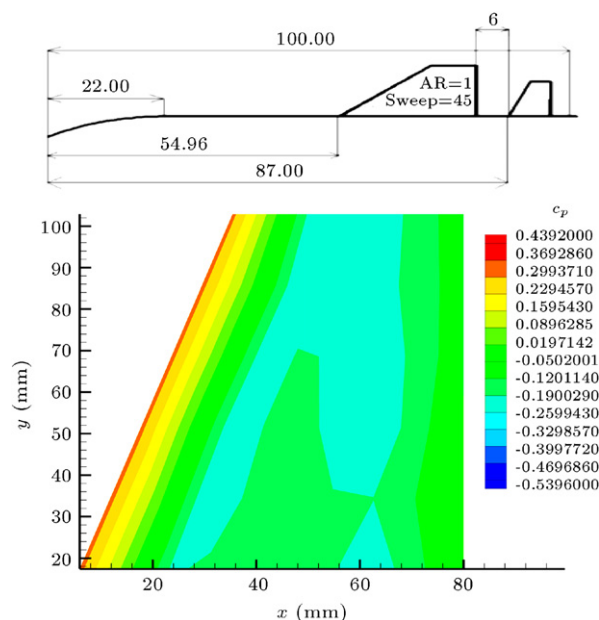
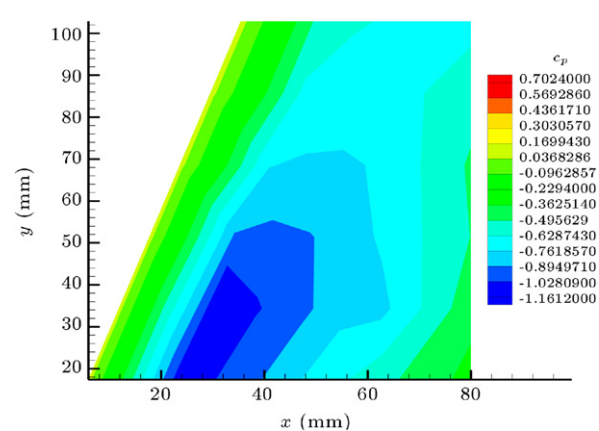
(a) $\alpha = 5^\circ$.(b) $\alpha = 30^\circ$.

Figure 4: The flowfield behind the TW3 configuration.

Note that TW5 and TW3 both have a wing aspect ratio of 1.0, with different wing sweep angles. According to Figure 6(c), at this high angle of attack, two vortices are formed downstream of the wing; the outboard one is the wing tip vortex whose effect on the tail is not so strong due to the high wing aspect ratio and high wing to tail span ratio, and the inboard one is the body vortex, which has rolled up in the vicinity of the tail leading edge. The latter has a strong effect on the tail and, as observed in Figure 6(d), the suction zone on the tail upper surface is situated near the tail root at the junction of the tail and body. The nose and forebody vortex effect are observed in the form of a small region at the top of the body vortex zone in the velocity profile shown in Figure 6(c).

Note that the wing signature on the tail at $\alpha = 30^\circ$ for TW5 is slightly different from that for TW3 at the same angle of attack, due to their different wing sweep angles. As pointed out earlier, for TW3 with higher swept wing, the tip vortex effects are more pronounced, that is the suction zone for this configuration is more extended towards the tail tip, due to stronger wing tip vortex effects.

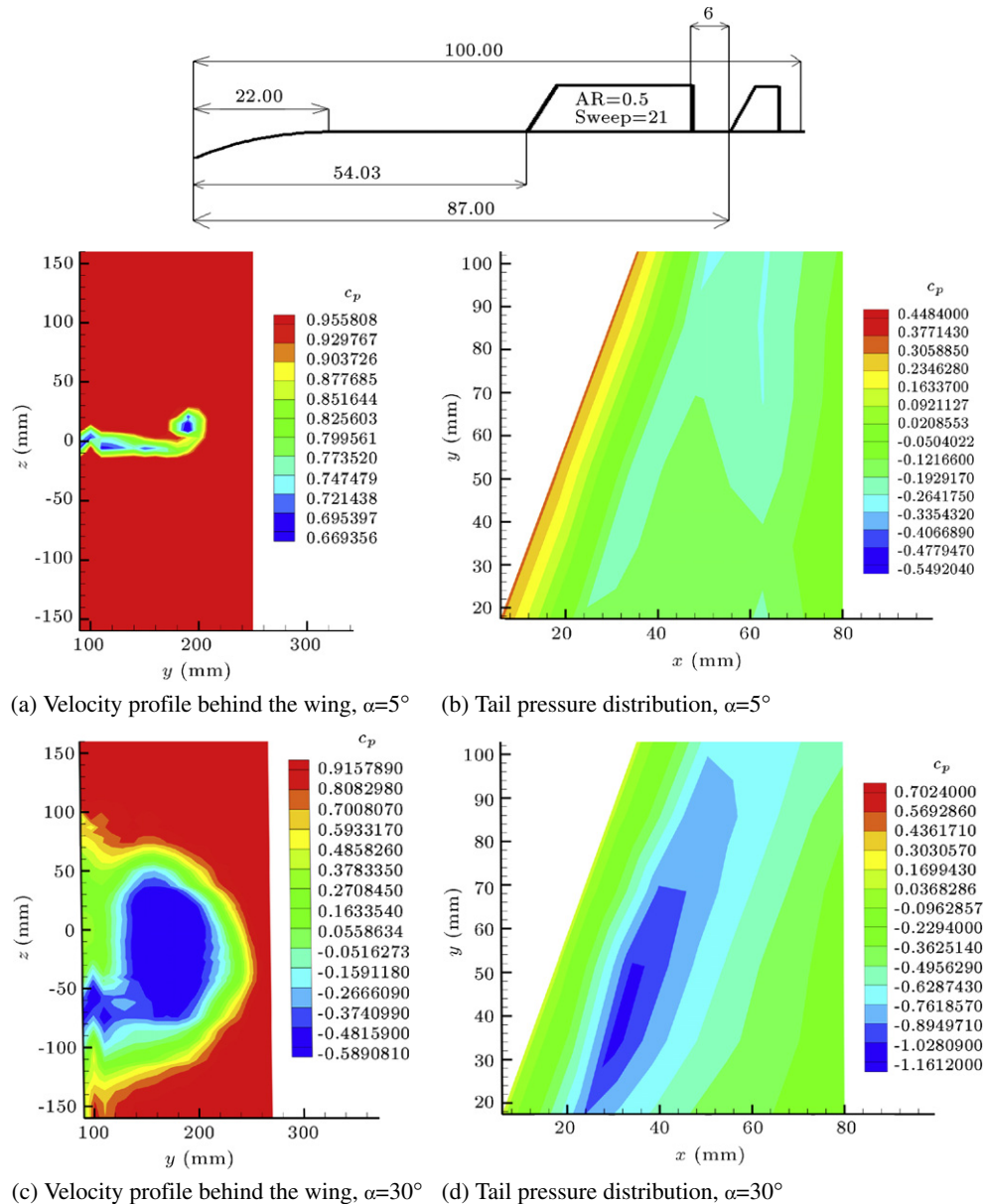


Figure 5: The flowfield behind the TW4 configuration.

Figure 7 summarizes the effects of wing geometric parameters on the chord wise pressure distribution of the tail at a 5° angle of attack for two span wise sections; $y/b = 0.28$ and $y/b = 0.71$. For both cases, as can be seen, the presence of the wing, regardless of its shape, decreases the suction peak, thus decreasing the lift force on the tail.

Further, the sectional pressure distribution, at $y/b = 0.71$, shows a second suction peak near $x/c = 0.8$, an indication of the tail tip vortex. This suction peak is not observed at $y/b = 0.28$ (Figure 7(a)), because the tip vortex effects at an angle of attack of 5° , are not strong enough to affect the regions far from the tip.

At 30° angles of attack, according to Figure 8, this trend is reversed. All wings considered in the present experiments exhibit a favorable effect on the tail and increase the suction peak of the tail surface, which remarkably increases the tail effectiveness at high angles of attack. This behavior is shown to be independent of wing geometric parameters.

An interesting feature of Figure 8 is the different pressure distributions on the tail downstream of each wing. For both span wise sections, the configurations, TW1, TW2 and TW4, exhibit a different behavior, i.e. a single suction peak near $x/c = 0.4$ and pressure recovery throughout the remainder of the tail. For TW3 and TW5, the behavior is similar to that of the *T* configuration, which has a nearly constant suction zone throughout the upper surface. Note from Table 1 that configurations with low aspect ratio wings, i.e. TW1, TW2 and TW4, have a sharp single pressure peak on the tail, while the configurations with a wing aspect ratio of unity have a relatively flat suction zone in the tail pressure distribution.

As explained earlier, for the configurations with a low aspect ratio wing, the wing tip vortex effect is directly felt at the tail outboard positions, while for higher aspect ratio wing configurations, the tail is completely exposed to the wake of the wing with small favorable effects, due to body/nose vortex shedding and the tail tip vortex. According to Figure 8(a) and

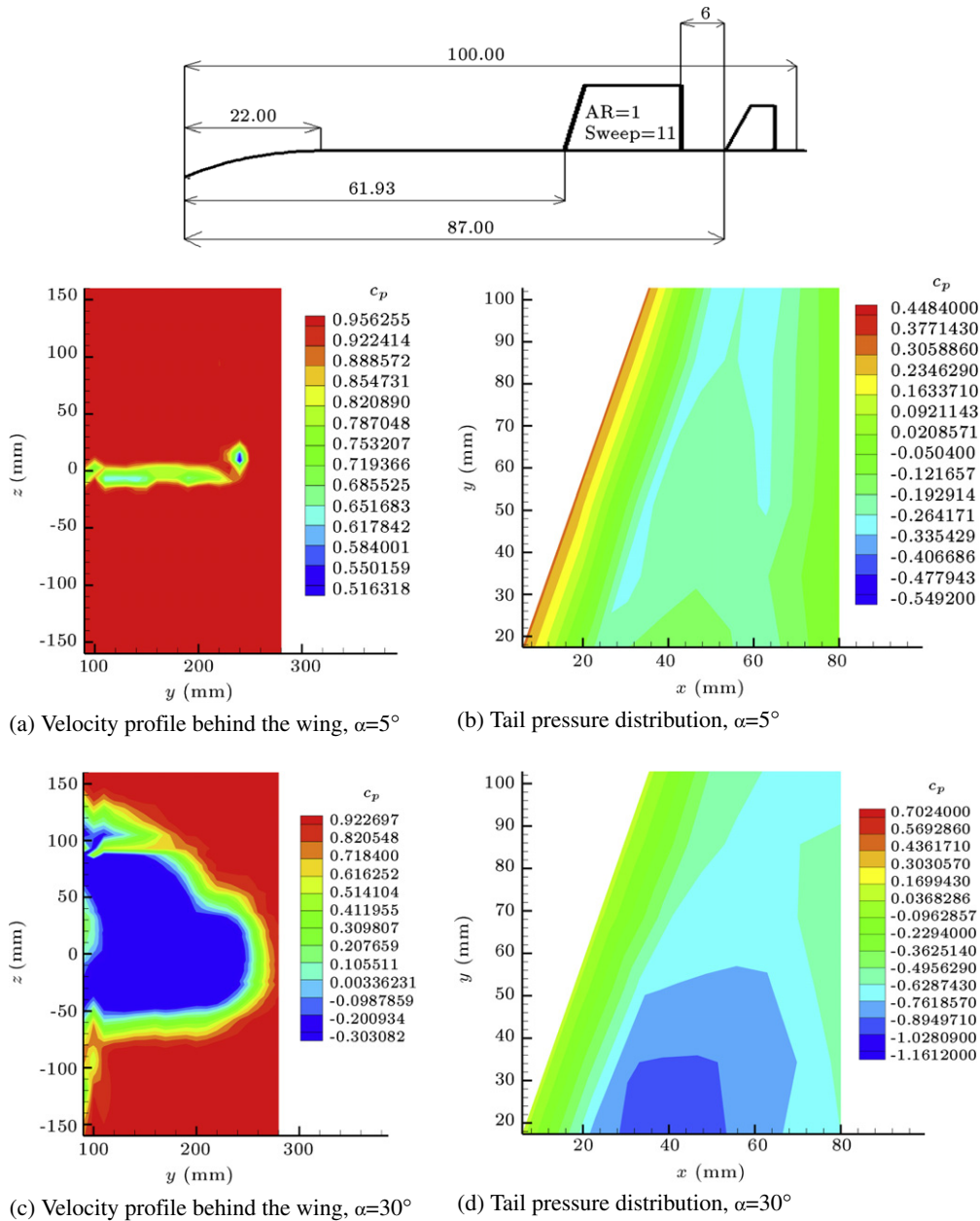


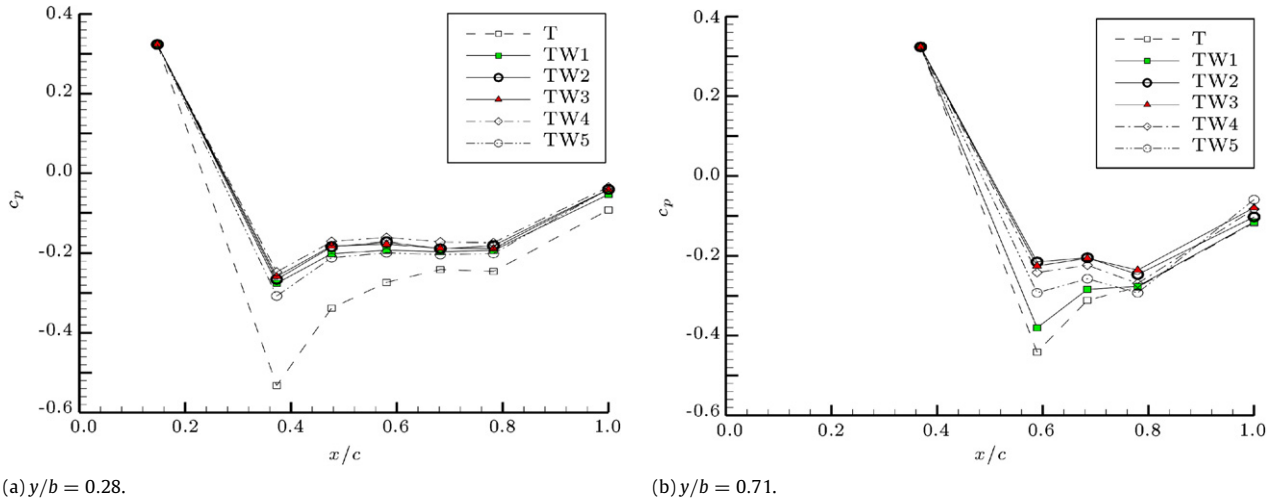
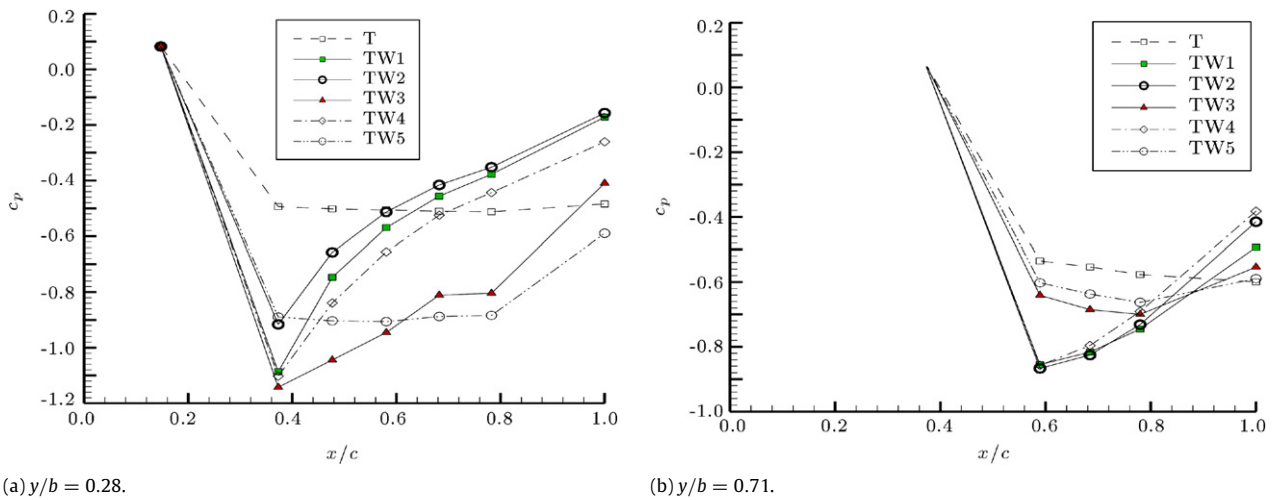
Figure 6: The flowfield behind the TW5 configuration.

(b), the tail pressure distribution for high aspect ratio wing configurations, TW3 and TW5, are similar to the body–tail alone, *T*, configuration. Both the high aspect ratio wing configuration and the tail alone configuration take advantage of nose/body vortex shedding and the tail tip vortex at high angles of attack, while for the lower aspect ratio wing configurations, the tail is exposed to the wing tip vortex. Also in addition to vortex shedding and the tail tip vortex, the wing tip vortex also gives rise to a suction peak and enhances the lift force developed on the tail.

4. Conclusion

Extensive wind tunnel tests were conducted on several wing–tail combinations to study the effects of wing geometric parameters on the flow field over the tail. The results show

that, no matter what the wing geometry is, the flow over the tail is deteriorated by the presence of the wing at low angles of attack, where the flow over the tail alone configuration is completely attached. At high angles of attack, where the tail alone flow separates from the surface, the vortices developed on wing and body re-attach the separated flow and enhance tail effectiveness at high incidence. However, the way the wing and body vortices affect tail flow strongly depends on wing geometry. The present results reveal that two factors are responsible for wing–tail interactions; wing tip/leading edge vortex and nose/body vortex. Wing tip vortex effects appear on the tail outboard position, extending in the span wise direction, while the body vortex signature on the tail is mostly concentrated on the tail inboard position and extends in the chord wise direction. The wing aspect ratio is a dominant factor on tail flow; for low aspect ratio wings, the wing tip/leading

Figure 7: Chord wise pressure distribution on the tail at $\alpha = 5^\circ$.Figure 8: Chord wise pressure distribution on the tail at $\alpha = 30^\circ$.

edge vortex signature at high angles of attack can be clearly seen on the tail outboard with the small effect of body vortex on the inboard section of the tail. For a wing aspect ratio of unity, wing tip vortex effects on the tail are not so important, and the dominant factor is the body vortex, which appears at the tail inboard extending in the chord wise direction.

References

- [1] Wieselsburger, C. "Airplane body (non-lifting system) drag and influence on lifting system influence of the airplane body on the wings", in W.F. Durand, Ed., *In Aerodynamics Theory*, IV, Chap. III., Sec. 1, pp. 152–157, Julius Springer, Berlin (1934).
- [2] Hopkins, E.J. and Carel, H.C. "Experimental and theoretical study of the interference at low speed between slender bodies and triangular wings", NACA RM A53A14 (1953).
- [3] Nielson, J.N. and Pitts, W.C. "Wing-body interference at supersonic speeds with an application to combinations with rectangular wings", NACA TN-2677 (1952).
- [4] Ferrari, C. "Interference between wing and body at supersonic speeds—theory and numerical application", *Journal of Aeronautical Sciences*, 15(6), pp. 317–336 (1948).
- [5] Morikawa, G.K. "The wing-body problem for linearized supersonic flow", Ph.D. Thesis, Calif. Inst. of Tech. (1949).
- [6] Silverstein, A. "Toward a rational method of tail-plane design", *Journal of Aeronautical Sciences*, 6(9), pp. 361–369 (1939).
- [7] Silverstein, A. and Katzoff, S. "Design charts for predicting downwash angles and wake characteristics behind plain and flapped wings", NACA Rep. 648 (1939).
- [8] Morikawa, G.K. "Supersonic wing-body-tail interference", *Journal of Aeronautical Sciences*, 10(5), pp. 333–340 (1952).
- [9] Lomax, H. and Byrd, P.F. "Theoretical aerodynamic characteristics of a family of slender wing-tail-body combinations", NACA TN 2554 (1951).
- [10] Lagerstrom, P.A. and Graham, M.E. "Aerodynamic interference in supersonic missiles", In *SM-13743*, Douglas Aircraft Co., Inc. (1950).
- [11] Brebner, G. "The control of guided weapons", AGARD LS-85 (1976).
- [12] Lesieutre, D.J., Mendenhall, M.R., Nazario, S.M. and Hemsch, M.J. "Aerodynamic characteristics of cruciform missiles at high angles of attack", AIAA 87-0212 (1987).
- [13] Lesieutre, D.J., Dillenius, M.F.E. and Whittaker, C.H. "M3F3CA aerodynamic analysis for finned vehicles with axisymmetric bodies", NEAR TR-424 (1991).
- [14] Lesieutre, D.J., Love, J.L. and Dillenius, M.F.E. "High angle of attack missile aerodynamics including rotational rates-program M3HAX", AIAA 96-3392 (1996).
- [15] Lesieutre, D.J., Love, J.L., Dillenius, M.F.E. and Blair, A.B. "Recent applications and improvements to the engineering level aerodynamic prediction software" MISL3, AIAA 2002-0275 (2002).
- [16] Abney, E. "High angle of attack aerodynamic predictions using missile edatcom", AIAA 2005-5086 (2005).

Ali R. Davari is Assistant Professor in the Department of Mechanical and Aerospace Engineering at the Islamic Azad University, the Science and Research Campus in Iran. He graduated with a Ph.D. degree in 2006 and has published over 11 journal papers. He has conducted several experimental studies on Unsteady Aerodynamics and Interference Effects. He is also interested in

New Prediction and Optimization Methods in Aerodynamics, such as Neural Networks and Evolutionary Algorithms.

Mohammad Reza Soltani, Professor in the Aerospace Engineering Department of Sharif University of Technology, Tehran, has a Ph.D. in Aerodynamics from the University of Illinois at Urbana-Champaign, USA. His research interests include Applied Aerodynamics, Unsteady Aerodynamics Wind Tunnel Testing, Wind Tunnel Design and Data Processing.

Farshid Askari graduated with B.S. and M.S. degrees in Aerospace Engineering and Aerodynamics from Sharif University of Technology, Iran, where since 2010 he has also been pursuing his Ph.D. degree course in Aerospace Engineering. His research interests include Applied Aerodynamics, Unsteady Aerodynamics Wind Tunnel Testing and Data Processing.

H.R. Pajuhand. His/her biography was not available at the time of publication.